Optics Letters

Quantum anomalous Hall-quantum spin Hall effect in optical superlattices

Ce Shang,[1,2,4] Xianfeng Chen,[1,2] Weidong Luo,[3] and Fangwei Ye[1,2,*]

[1]The State Key Laboratory of Advanced Optical Communication Systems and Networks, School of Physics and Astronomy, Shanghai Jiao Tong University, Shanghai 200240, China
[2]Key Laboratory for Laser Plasma, Collaborative Innovation Center of IFSA, Shanghai Jiao Tong University, Shanghai 200240, China
[3]Key Laboratory of Artificial Structures and Quantum Control, Shanghai Jiao Tong University, Shanghai 200240, China
[4]e-mail: shangce1989@sjtu.edu.cn
*Corresponding author: fangweiye@sjtu.edu.cn

Received 7 November 2017; revised 6 December 2017; accepted 10 December 2017; posted 11 December 2017 (Doc. ID 312961); published 9 January 2018

We consider the topological characteristics of the spin-orbital coupling particles loaded in one-dimensional (1D) optical superlattices subject to the Zeeman field. The phase shift of the superlattice provides a virtual dimension which allows us to simulate two-dimensional topological phases with a physically 1D system. The system possesses a variety of quantum phase transitions over a large parametric space and two important topological phases, namely, quantum anomalous Hall (QAH) and quantum spin Hall (QSH) phases are found to coexist in the system, but they reside in different bandgaps. This new category of gap-dependent QAH–QSH insulator paves the way for the possible observation of the coexistence of QSH and QAH effects at one platform.

OCIS codes: (020.0020) Atomic and molecular physics; (020.7490) Zeeman effect; (020.1475) Bose-Einstein condensates.

https://doi.org/10.1364/OL.43.000275

The quantum spin Hall (QSH) effect [1–4] and quantum anomalous Hall (QAH) effect [5,6] are both fundamental transport processes arising from the nontrivial topological order. Traditionally, a QSH insulator is considered to be protected by the time-reversal-symmetry (TRS), with a pair of spin-polarized states counter-propagating on the sample edge. In contrast, the QAH effect requires the breaking of TRS, which is induced by internal magnetization and spin orbital coupling (SOC). The mechanisms of QSH and QAH are separately well established; however, manifesting these two topological effects simultaneously in one system is rather difficult, due to the dilemma of protecting or breaking TRS. Nevertheless, a very recent investigation reveals that a QSH state could survive in a TRS-broken system [7] until the exchange field is over a critical value, at which the bulk bandgap closes and reopens. The discovery of this TRS-broken QSH effect conquers the difficulty of presenting a QSH and QAH state in one device.

Ultracold atoms in optical lattices are widely used in condensed matter physics to investigate the strongly correlated many-body interaction processes [8,9] and topological insulators [10,11]. When particles are loaded in the optical potential with a commensurate or incommensurate period, the system may possess a topological insulator phase such that localized edge states occur within the bandgap [12,13]. Furthermore, the realization of the effective SOC in cold atoms [14–16] and the dynamics of spin particles in the Zeeman field [17,18], as the readily modified parameters, open intriguing possibilities to control the versatile topological phases with more adjustable degree of freedoms. Although the topological phases are thought to be limited in two-dimensional (2D) systems [19,20], it has been shown both theoretically and experimentally that one-dimensional (1D) optical potentials support such topological properties [21–23]. Thus, a 1D system offers a very simple, yet powerful, means to probe the topological phases of the higher-dimension systems, and the reduction of the dimension simplifies the experimental designs [24]. Motivated by these progresses, here we propose an applicable platform to investigate QSH and QAH by trapping spin particles in 1D optical lattice subject to the Zeeman field.

Thus, we show in this Letter a quantum anomalous Hall-quantum spin Hall (QAH-QSH) insulator, namely the coexistence of QAH and QSH in a 1D optical superlattice. The superlattice is characterized by a phase shift that acts as a virtual dimension such that the 1D structure could be mapped onto a 2D system with intriguing topological edge states. Different from the previously reported quantum spin-quantum anomalous Hall insulator, where the QAH and QSH occur within the same bandgap [25,26], the QAH and QSH in our system are found to occur in separated bandgaps, namely gap-dependent, by which our scheme avoids the particle energy degeneracy and makes it more feasible for the possible experimental observation.

We consider trapping spin particles in 1D optical potentials, with the Hamiltonian described by

$$H = -t\sum_{i,\sigma} c_i^{\sigma\dagger} c_{i+1}^{\sigma} + \sum_{i,\sigma}^{N} V_i c_i^{\sigma\dagger} c_i^{\sigma} + i\lambda\sum_{i,\alpha\beta} \sigma_y \left(c_i^{\alpha\dagger} c_{i+1}^{\beta} - c_i^{\alpha\dagger} c_{i-1}^{\beta}\right) - \Omega\sum_{i,\sigma} c_i^{\sigma\dagger}\sigma_z c_i^{\sigma}, \quad (1)$$

with

$$V_i = V\cos(2\pi\omega i + \delta). \quad (2)$$

Here N is the number of the lattice sites, σ_y and σ_z are Pauli matrices, V is the potential strength with the rational period $1/\omega$, δ is the phase shift accounting for displacement of the potential, the operators $c_i^{\sigma\dagger}$, c_i^{σ} ($\sigma = \alpha, \beta$. α, β denotes the spin-up and spin-down component, respectively) are the creation and annihilation spin-dependent operators with spin σ on the ith sites, the hopping amplitude between the nearest cites t is set to be the unity ($t = 1$), Ω characterizes Zeeman splitting, and λ is the strength of the SOC term. The basic scheme is shown in Fig. 1. In the following, we assume that the nth eigenstate of the spinor is given by $|\psi_n^{\sigma}\rangle = \sum_i u_{i,n}^{\sigma} c_{i\sigma}^{\dagger}|0\rangle$, such that the original eigenvalue equation $H|\psi_n^{\sigma}\rangle = E_n|\psi_n^{\sigma}\rangle$ is now represented by two coupled Harper equations:

$$-(u_{i+1,n}^{\alpha,\beta} + u_{i-1,n}^{\alpha,\beta}) + [V\cos(2\pi\omega i + \delta) \mp \Omega]u_{i,n}^{\alpha,\beta} \pm \lambda(u_{i+1,n}^{\beta,\alpha} - u_{i-1,n}^{\beta,\alpha}) = E_n^{\alpha,\beta} u_{i,n}^{\alpha,\beta}, \quad (3)$$

where $u_{i,n}^{\sigma}$ is the amplitude of the spin particle wave function at the ith site with V_i the on-site diagonal potential, and E_n^{σ} denotes the nth spin particle eigenenergy. For simplicity, we only consider $V_i = V\cos(2\pi\omega i + \delta)$ with rational $\omega = p/q$ (p, q are integers prime to each other), i.e., a commensurate potential so that the Bloch theory applies to the particle states. For such periodic potential, the wave functions have the Bloch form $u_{i+q}^{\sigma} = e^{ikq} u_i^{\sigma}$. Considering the Bloch state $u_j^{\sigma} = e^{ikj}\phi_j^{\sigma}(k)$ for $|k| \le \pi/q$, Eq. (3) can be derived as

$$-(e^{ik}\phi_{j+1}^{\alpha,\beta} + e^{-ik}\phi_{j-1}^{\alpha,\beta}) + [V\cos(2\pi\omega i + \delta) \mp \Omega]\phi_j^{\alpha,\beta} \pm \lambda(e^{ik}\phi_{j+1}^{\beta,\alpha} - e^{-ik}\phi_{j-1}^{\beta,\alpha}) = E(k)\phi_j^{\alpha,\beta}. \quad (4)$$

On account of $\phi_{j+q}^{\sigma}(k) = \phi_j^{\sigma}(k)$, solving the harper equation [Eq. (4)] can be simplified by solving the eigenvalue equation $M\Phi = E\Phi$, where $\Phi = (\phi_1^{\alpha}, \cdots, \phi_q^{\alpha}, \phi_1^{\beta}, \cdots, \phi_q^{\beta})^T$ and M is a $2q \times 2q$ matrix. The band splits into $2q$ subbands, corresponding to $2q - 1$ bulk energy gaps. Under the open boundary condition, we find that the edge states emerge in the bandgaps. The number of the edge states in the gap regime is defined by the gap Chern number [27], which will be introduced in the next section.

As seen from Eq. (4), the 1D superlattice itself has two good quantum numbers k and δ; mathematically, the equation describing this 1D model is essentially equivalent to the Harper equation describing the electron hopping in a 2D periodic potential in a uniform magnetic field [28], except that the role of k_y in that true 2D system is played by δ in 1D chain. Since a Chern number can characterize that 2D system, then, formally, a Chern number can also characterize our system. The edge states generally arise at the boundary of the bulk systems of the nontrivial topological phase, and the number of edge states is directly linked to the gap Chern number, a topological invariant that involves integration over the occupied bands in the momentum space. An effective Brillouin zone with respect to the Bloch vector k and potential shift δ (a virtual dimension) forms a T^2 torus. Adiabatically varying δ and k on the torus, one gets a manifold of Hamiltonian $H(k, \delta)$ in the parametric space. For the eigenstates $\phi(k, \delta)$ of the Hamiltonian $H(k, \delta)$, the Berry connection is defined as $A_{k,\delta} = i\langle\phi(k, \delta)|\partial_{k,\delta}|\phi(k, \delta)\rangle$. The Chern number of the mth bandgap C^m is given as the sum of the Chern numbers of the occupied bands [21,29]:

$$C^m = \frac{1}{2\pi}\sum_{n=1}^{m}\int_0^{2\pi/q} dk \int_0^{2\pi} d\delta(\partial_k A_\delta - \partial_\delta A_k). \quad (5)$$

However, matrix σ_z in the Hamiltonian [Eq. (1)] breaks the spin SU(2) symmetry. The Bloch Hamiltonian $H(k, \delta) = H_+(k, \delta) \oplus H_-(k, \delta)$ displays the upper and lower bands separated by an insulating gap, where $H_\pm(k, \delta)$ denotes the fiber bundle slashed into two nontrivial parts. As a consequence, the definition of the Chern number in Eq. (5) is invalid to represent the number of edge states, because spin operator s_z is no longer a good quantum number due to spin mixing caused by the SOC term and Zeeman field [30]. To calculate the spin Chern number, we follow the procedure [30,31], where matrix $\hat{\sigma}_z$ is constructed and diagonalized for the occupied states $\langle\phi_m(k, \delta)|\hat{\sigma}_z|\phi_n(k, \delta)\rangle$ (m, n are the band indices of occupied states at each k and δ). Here, we use the spin-up or spin-down eigenvectors $|\psi^{\pm}\rangle$ of the matrix $\hat{\sigma}_z$, which denote the occupied states projected into the spin-up and spin-down manifolds as $\phi^{\pm}(k, \delta) = \langle\psi^{\pm}(k, \delta)|\phi(k, \delta)\rangle$. In addition, we can define the corresponding Berry connection $A_{k,\delta}^{\pm} = i\langle\phi^{\pm}(k, \delta)|\partial_{k,\delta}|\phi^{\pm}(k, \delta)\rangle$, and the spin-up and spin-down Chern number $C_{\pm}^m$. Note that such defined Chern number $C_{\pm}^m$ is a topological invariant, as it is robust against continuous deformations of the Hamiltonian. Hence, the spin Chern number [25] $C_s^m = \frac{1}{2}(C_+^m - C_-^m)$ is a well-defined topological invariant [32]. However, neither C^m or C_s^m can make a complete description of the topological property in our system. Therefore, the topological invariants are codetermined by combining C^m and C_s^m as a Chern number pair (C^m, C_s^m) [33]. Corresponding to the bulk-edge corresponding theory, the first number of the Chern number pair, C^m, denotes the counts of the chiral edge states with the same propagation direction in the mth bandgap, and the second number C_s^m of the Chern number pair represents the number of the helical edge states. Therefore, $(C^m, C_s^m) = (C^m \neq 0, 0)$ represents the QAH phase, where chiral edge states (the number of which is $|C^m|$) appear, whereas $(C^m, C_s^m) = (0, 1)$ represents QSH phase where helical edge states emerge. Of course, $(C^m, C_s^m) = (0, 0)$ represents a normal insulate (NI) phase where no types of edge states exist. Hence, such a definition of the Chern number pair provides a complete description on the topological properties of each bandgap in our system.

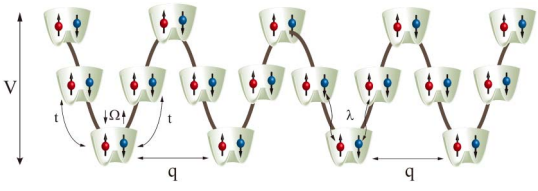

Fig. 1. Schematic layout of the potential and coupling fields. An ultracold gas of spin particles (blue and red balls) is prepared in a 1D optical lattice with a period q and a depth V. A spin-independent, staggered, Zeeman field Ω detunes one particle of the spin pair from the other. The hopping term t and the SOC term λ represent the interactions between the nearest spin pairs.

The dependence of the energy spectrum of Hamiltonian [Eq. (1)] on potential period $\omega = p/q$ (limited in the [0,1] interval) is shown in Fig. 2, which shows a butterfly-like structure. Note that the spectrum exhibits a multigap structure, resulting from the combined actions of the underlying quasiperiodic potential, Zeeman field, and SOC effects. Interestingly, near the period $\omega = 1/3$, one additional gap emerges (indicated with the red square in Fig. 2). As will be discussed below, this additional gap is of the QSH phase, while the other two lower or two upper gaps are of QAH phases. We should mention that the number/size of these gaps and topological properties could be readily tuned by the SOC and Zeeman field amplitude.

Figure 3 presents the band structure of the commensurate potential under the open boundary condition against the virtual dimension δ. Without loss of the generality, here we present our idea on the intuitively most transparent case at $\omega = 1/3$ and vary δ from 0 to 2π. The lines connecting

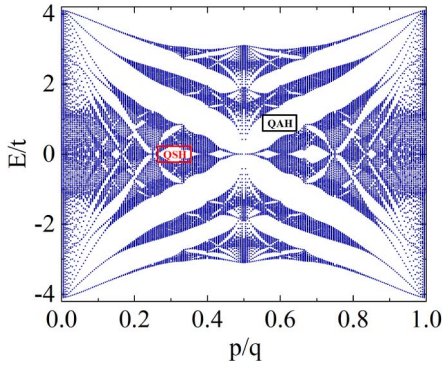

Fig. 2. Butterfly energy spectra with respect to potential period $\omega = p/q$ varying from 0 to 1 under a periodic boundary condition, here potential depth $V = 1.5$, the number of sites $N = 200$, SOC term $\lambda = 0.6$, and Zeeman field strength $\Omega = 0.6$. (Dimensionless units are used throughout this Letter.) The blank areas with wing shapes represent the bandgap regimes. The blank area in the red square indicates the QSH phase, while the other gaps stand for QAH phases.

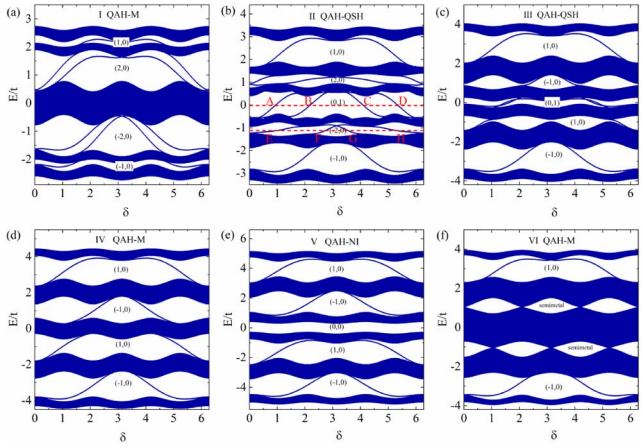

Fig. 3. Energy spectra versus phase δ under open boundary condition at potential depths $V = 1.5$, SOC term $\lambda = 0.3$, and period $\omega = 1/3$. From (a) to (e): Zeeman field $\Omega = 0.3, 1.0, 1.6, 2.0, 2.7$. The numbers in the brackets denote the Chern number pair for the respective bandgaps. (f) Semi-metal phase with the parameters $\lambda = 0.58$ and $\Omega = 1.5$.

the separated bands in Fig. 3 are the evidence of the edge states. With the variation of the Zeeman field strength Ω, some bands collapse, undergo a metal (M) phase, and then reopen, leading to a phase transition of the associated gap. Such a phase transition is well captured by the variation of either component in the Chern number pair (C^m, C_s^m), as indicated in each gap in Fig. 3. Obeying the bulk-edge correspondence principle, the change of Chern number is accompanied with the emergence or elimination of specific edge states, as seen in Fig. 3. To be specific, considering the Chern number pair for the third and fourth (or second) gap, in Fig. 3(b) and Fig. 3(e), respectively, (C^4, C_s^4) changes from (2, 0) in Fig. 3(b) to (−1, 0) in Fig. 3(e), corresponding to the number of chiral states changing from 2 to 1. (Here the sign of the Chern number stands for the propagation direction of the associated edge state along the virtual dimension.) Meanwhile, (C^3, C_s^3) changes from (0, 1) into (0, 0), corresponding to the pair of helical states changing from 1 into 0. The Chern number pair for the first and fifth gaps remains unchanged from Figs. 3(b)–3(e), telling that the topological phases for these two gaps are maintained, as evidenced by the preservation of one chiral edge state. Finally, we mention that the transition phase could be either metal or semi-metal. The latter occurs when the gap closes at some critical point of the potential phase shift; see one example in Fig. 3(f), where two pairs of neighbor band touch each other at Dirac points.

The aforementioned identification in the topological phase for each gap fully coincides with the characteristics of their associated edge states. For example, in the gap of a QSH phase, as shown in Fig. 3(b), there exist four different edge modes labeled by A, B, C, and D. Modes A and C reside at the right boundary of the superlattice, while modes B and D reside at the left boundary [Fig. 4(a)]. One finds that the edge states at the same boundary feature opposite spin-polarization and opposite group velocity with respect to the virtual dimension δ. The existence of such a pair of helical edge states is a hallmark of QSH. In contrast, in the gap of a QAH phase, at the same boundary edge, modes propagate toward one direction (no counter-propagating modes occur at the same boundary) [Fig. 4(b)]. By varying the parameter δ and performing spin-resolved density measurements [34], the corresponding topological phase can be identified.

Not only can the Zeeman field readily tune the topological phase of the structure as discussed above, but also the SOC provides an equally efficient way for their phase control. To clarify the intrinsic richness of topological phase transitions,

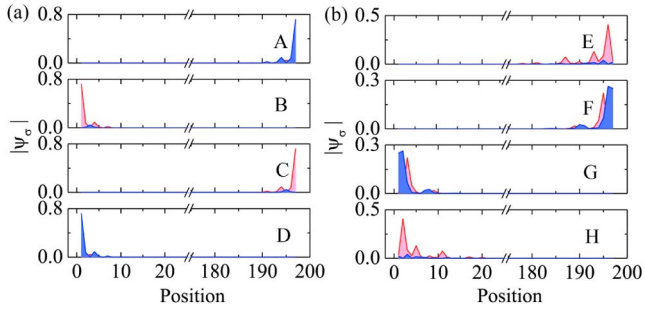

Fig. 4. Eigenmode profile corresponding to the labels denoted on the red dashed line in Fig. 3(b), for a QSH phase (left panel) and a QAH phase (right panel). The red and blue lines represent the spin-up and spin-down component, respectively.

we introduce a phase diagram that contains topological phases associated to all the bulk gaps. The influence of the interplay between the Zeeman field and the SOC strength on the topological phase is systematically shown in Fig. 5. In this figure, $V = 1.5$ and $\omega = 1/3$ are fixed, and (C^m, C_s^m) is calculated in the interval of $\lambda \in [0, 1]$ and $\Omega \in [0, 3]$. According to the specific values of (C^m, C_s^m), the plane of (λ, Ω) is divided into five different topological phase regimes: QAH – $M_{1,2}$, QAH – $QSH_{1,2}$, and QAH–NI, and each of them is bounded by a metal or semi-metal phase. The transition between these five topological phases can be achieved by tuning λ and Ω. For example, the phase transition shown from Figs. 3(a)–3(e) is realized by the increasing of Ω with a fixed $\lambda = 0.3$, as indicated with a dashed line in Fig. 4. However, in general, both Zeeman and SOC could be used to tune the topological phase. As shown in area I in Fig. 5, the system is in a QAH – M_1 phase with a metallic phase in the intermediate region, where the Zeeman term is not strong enough to break the degeneracy of the central bands. The system manifests QAH – QSH_1 states in area II, which sandwiches the QSH state in the two upper and lower band QAH states, with the topological invariants $[(-1, 0), (-2, 0), (0, 1), (2, 0), (1, 0)]$. The phase of the III(IV) case is very similar to those of the II(I) case, except for the change of topological invariants in the QAH regime. In the area V, the midgap contains no edge states: it is topologically equivalent to a QAH-NI.

In this Letter, we use a 1D superlattice to load the spin-orbit coupling particles subject to the Zeeman field and, by virtue of the virtual dimension provided by the phase shift of the superlattice, we are able to simulate the 2D topological phases in physically 1D systems. A novel butterfly-like spectrum and intriguing topological phase transitions are found to occur, when one tunes the spin-orbital coupling strengths or the Zeeman field. Especially interesting is that we find a new category of topological phase, named QAH–QSH insulator, where the QAH phase and QSH phase coexist in the same system. In contrast to the previously reported results [25,26], where these two important topological phases locate in the same bandgap, our scheme locates them in different bandgaps, thus avoiding their energy degeneracy and making the scheme more attractive for the experimental observation. Finally, we notice that very recent experimental platforms have been put forward in an optical lattice [35] that might be used to implement our theoretical proposal, and our proposal may also be realized in a synthetic frequency dimension [36]. Manipulating the spin polarized edge states, by altering the topological phases we revealed in this Letter, may offer a novel route to realize the spin-based quantum computation.

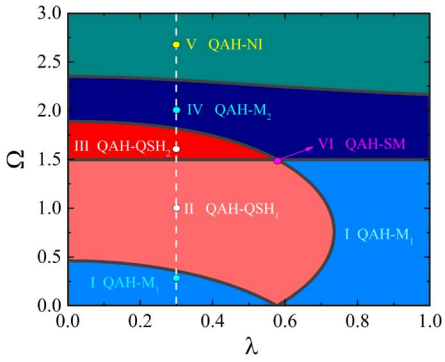

Fig. 5. Phase diagram in the (λ, Ω) plane. The heavy lines represent the phase boundaries, where some part of the system becomes metallic. The vertical dashed line represents the phase transition process with the increase of Ω. The color circles represent the parametric points whose corresponding band spectra are shown in Fig. 3.

Funding. National Natural Science Foundation of China (NSFC) (11474197, 11521404, U1632272; 61475101); National Basic Research Program of China (2013CB921902).

REFERENCES

1. B. A. Bernevig and S.-C. Zhang, Phys. Rev. Lett. **96**, 106802 (2006).
2. C. L. Kane and E. J. Mele, Phys. Rev. Lett. **95**, 226801 (2005).
3. B. A. Bernevig, T. L. Hughes, and S.-C. Zhang, Science **314**, 1757 (2006).
4. X. Zhou, Z. Xiao, H. Luo, and S. Wen, Phys. Rev. A **85**, 043809 (2012).
5. C.-X. Liu, X.-L. Qi, X. Dai, Z. Fang, and S.-C. Zhang, Phys. Rev. Lett. **101**, 146802 (2008).
6. R. Yu, W. Zhang, H.-J. Zhang, S.-C. Zhang, X. Dai, and Z. Fang, Science **329**, 61 (2010).
7. Y. Yang, Z. Xu, L. Sheng, B. Wang, D. Xing, and D. Sheng, Phys. Rev. Lett. **107**, 066602 (2011).
8. T. Stöferle, H. Moritz, C. Schori, M. Köhl, and T. Esslinger, Phys. Rev. Lett. **92**, 130403 (2004).
9. L.-M. Duan, E. Demler, and M. D. Lukin, Phys. Rev. Lett. **91**, 090402 (2003).
10. X.-L. Qi and S.-C. Zhang, Rev. Mod. Phys. **83**, 1057 (2011).
11. M. Z. Hasan and C. L. Kane, Rev. Mod. Phys. **82**, 3045 (2010).
12. L. Fallani, J. Lye, V. Guarrera, C. Fort, and M. Inguscio, Phys. Rev. Lett. **98**, 130404 (2007).
13. G. Roati, C. Derrico, L. Fallani, M. Fattori, C. Fort, M. Zaccanti, G. Modugno, M. Modugno, and M. Inguscio, Nature **453**, 895 (2008).
14. X.-J. Liu, M. F. Borunda, X. Liu, and J. Sinova, Phys. Rev. Lett. **102**, 046402 (2009).
15. L. W. Cheuk, A. T. Sommer, Z. Hadzibabic, T. Yefsah, W. S. Bakr, and M. W. Zwierlein, Phys. Rev. Lett. **109**, 095302 (2012).
16. Y.-J. Lin, K. Jimenez-Garcia, and I. Spielman, Nature **471**, 83 (2011).
17. X.-J. Liu, K. T. Law, T. K. Ng, and P. A. Lee, Phys. Rev. Lett. **111**, 120402 (2013).
18. N. Goldman, J. Budich, and P. Zoller, Nat. Phys. **12**, 639 (2016).
19. D. Thouless, Phys. Rev. B **27**, 6083 (1983).
20. L. Fu and C. L. Kane, Phys. Rev. B **74**, 195312 (2006).
21. L.-J. Lang, X. Cai, and S. Chen, Phys. Rev. Lett. **108**, 220401 (2012).
22. Y. E. Kraus, Y. Lahini, Z. Ringel, M. Verbin, and O. Zilberberg, Phys. Rev. Lett. **109**, 106402 (2012).
23. F. Mei, S.-L. Zhu, Z.-M. Zhang, C. Oh, and N. Goldman, Phys. Rev. A **85**, 013638 (2012).
24. O. Boada, A. Celi, J. Latorre, and M. Lewenstein, Phys. Rev. Lett. **108**, 133001 (2012).
25. M. Ezawa, Phys. Rev. B **87**, 155415 (2013).
26. T. Zhou, J. Zhang, B. Zhao, H. Zhang, and Z. Yang, Nano Lett. **15**, 5149 (2015).
27. S. A. Skirlo, L. Lu, Y. Igarashi, Q. Yan, J. Joannopoulos, and M. Soljačić, Phys. Rev. Lett. **115**, 253901 (2015).
28. D. R. Hofstadter, Phys. Rev. B **14**, 2239 (1976).
29. Q. Niu, D. J. Thouless, and Y.-S. Wu, Phys. Rev. B **31**, 3372 (1985).
30. E. Prodan, Phys. Rev. B **80**, 125327 (2009).
31. T. L. Hughes, E. Prodan, and B. A. Bernevig, Phys. Rev. B **83**, 245132 (2011).
32. D. Sheng, Z. Weng, L. Sheng, and F. Haldane, Phys. Rev. Lett. **97**, 036808 (2006).
33. M. Ezawa, Phys. Rev. Lett. **109**, 055502 (2012).
34. C. Weitenberg, M. Endres, J. F. Sherson, M. Cheneau, P. Schauss, T. Fukuhara, I. Bloch, and S. Kuhr, Nature **471**, 319 (2011).
35. S. Kolkowitz, S. Bromley, T. Bothwell, M. Wall, G. Marti, A. Koller, X. Zhang, A. Rey, and J. Ye, Nature **542**, 66 (2016).
36. L. Yuan, Y. Shi, and S. Fan, Opt. Lett. **41**, 741 (2016).